Role of Reversible Phase Transformation for Strong Piezoelectric Performance at the Morphotropic Phase Boundary

Hui Liu, Jun Chen, Houbing Huang, Longlong Fan, Yang Ren, Zhao Pan, Jinxia Deng, Long-Qing Chen, and Xianran Xing

Phys. Rev. Lett. **120**, 055501 — Published 29 January 2018

DOI: 10.1103/PhysRevLett.120.055501

Role of Reversible Phase Transformation for Strong Piezoelectric Performance at Morphotropic Phase Boundary

Hui Liu,[1] Jun Chen,[1,*] Houbing Huang,[2] Longlong Fan,[1] Yang Ren,[3] Zhao Pan,[1] Jinxia Deng,[1] Long-Qing Chen,[4] and Xianran Xing[1]

[1]Department of Physical Chemistry, University of Science and Technology Beijing, Beijing 100083, China

[2]Department of Physics, University of Science and Technology Beijing, Beijing 100083, China

[3]X-Ray Science Division, Advanced Photon Source, Argonne National Laboratory, Argonne, Illinois 60439, USA

[4]Department of Materials Science and Engineering, The Pennsylvania State University, University Park, Pennsylvania 16802, USA

*Corresponding author. junchen@ustb.edu.cn.

Abstract

A functional material with coexisting energetically equivalent phases often exhibits extraordinary properties such as piezoelectricity, ferromagnetism and ferroelasticity, which is simultaneously accompanied by field-driven reversible phase transformation. The study on the interplay between such phase transformation and the performance is of great importance. Here, we have experimentally revealed the important role of field-driven reversible phase transformation in achieving enhanced electromechanical properties using in-situ high-energy synchrotron X-ray diffraction combined with 2D geometry scattering technology, which can establish a comprehensive picture of piezoelectric-related microstructural evolution. High-throughput experiments on various Pb/Bi-based perovskite piezoelectric systems suggest that reversible phase transformation can be triggered by electric field at the morphotropic phase boundary and the piezoelectric performance is highly related to the tendency of electric-field-driven phase transformation. A strong tendency of phase transformation driven by electric field generates peak piezoelectric response. Further, phase-field modelling reveals that the polarization alignment and the piezoelectric response can be much enhanced by the electric-field-driven phase transformation. The proposed mechanism will be helpful to design and optimize the new piezoelectrics, ferromagnetics, or other related functional materials.

Modern functional materials such as piezoelectrics, ferromagnets, ferroelectrics, and ferroelastics, often display extraordinary responses to external stimuli at phase boundaries [1-5]. In such materials, external-stimuli-driven reversible phase transformations are extensively observed to be considered as a direct correlation to their extraordinary properties [4-10]. For example, excellent shape recovery properties, colossal magnetostriction, and giant magnetocaloric effect are accompanied by magnetic/temperature-field-driven phase transformation [6-8].

In cause of piezoelectrics, which are widely used for electromechanical devices, anomalously high piezoelectric performance is generally found at the position of morphotropic phase boundary (MPB), which was discovered more than half a century ago [11]. This discovery stimulated researchers to engineer and develop composition-controlled [12], pressure-induced [2,13], epitaxial strain-driven [1,5] MPB systems to achieve desirable properties, for examples, $Pb(Zr,Ti)O_3$-based (PZT) ceramics [12], $Pb(Mg_{1/3}Nb_{2/3})O_3$–$PbTiO_3$ (PMN-PT), $Pb(Zn_{1/3}Nb_{2/3})O_3$–$PbTiO_3$ (PZN-PT) single crystals [4,14], and $BiFeO_3$ thin films [1,5,15]. The MPB compositions typically exhibit electric-field-driven phase transformation as is observed for PZT [16], $PbTiO_3$-$BiScO_3$ [17], $(Bi_{1/2}Na_{1/2})TiO_3$-based ceramics [18-20], domain engineered PZN-PT single crystals [4], and $BiFeO_3$ thin films [1,5]. The theoretical studies [13,21,22], and in-situ diffraction experiments [23,24], have shed light on the role of field-driven phase transformation for the enhanced piezoelectric performance. Despite these advances, fundamental questions remain: What is the intrinsic correlation between electric-field-driven phase transformation and enhanced piezoelectricity? How does the phase transformation determine the piezoelectric performance at the MPB?

In this Letter, we perform in-situ high-energy synchrotron X-ray diffraction (SXRD) combined with 2D geometry scattering technology (see Fig. S1 of Supplemental Material [25]), which can simultaneously establish a comprehensive picture of piezoelectric-related structural evolution (lattice strain and phase transformation) and domain switching behavior under applied electric field [32-34]. First, piezoelectric related properties of domain switching, lattice strain, and phase

transformation evolution have been studied in two typical Pb/Bi-based MPB piezoceramics which have similar *c*/*a* ratios. One is the MPB composition of $0.64PbTiO_3$-$0.36BiScO_3$ (PT-36BS) with high piezoelectric performance, while the other is $0.38PbTiO_3$-$0.62Bi(Mg_{1/2}Ti_{1/2})O_3$ (PT-62BMT) with inferior performance. Subsequent the in-situ studies were extended to other Pb/Bi-based piezoelectric systems. It is interesting to find that the electric-field-driven phase transformation plays a general role to enhance the piezoelectric response. The ease of phase transformation results in better piezoelectric performance. Finally, the results from phase-field modelling confirm that the enhanced piezoelectric response stems from the improved polarization alignment via the electric-field-driven phase transformation. These results have implications for the fundamental understanding of the role of external stimuli driven phase transformation on related extraordinary properties and provide a possibility to design materials with enhanced piezoelectric response.

It has been established that the piezoelectric performance is directly correlated to the *c*/*a* ratio. Smaller *c*/*a* usually means higher mobility of domain walls and thus corresponds to enhanced piezoelectric properties [35,36]. However, despite PT-36BS (*c*/*a* = 1.02) [37], and PT-62BMT (*c*/*a* = 1.03) [38] exhibiting similar *c/a* rations, there is a stark contrast in their piezoelectric performance. PT-36BS exhibits a superior piezoelectric response (d_{33} = 430 pC/N) [37], while PT-62BMT shows an inferior one (d_{33} = 220 pC/N) [38]. The difference in their piezoelectric performance can also be clearly seen from the electric-field-induced strain (Fig. S2 of Ref. [25]). For instance, at E = 5 kV/mm, the positive strain is 0.29% and 0.14% for PT-36BS and PT-62BMT, respectively. It is worth exploring the nature of the huge difference in piezoelectric response. By using the present method of in-situ high-energy SXRD technology combined with appropriate 2D scattering geometry, the effect of electric field induced texture can be neglected at the 45° sector [32,33,39], which allows the reliable estimation of phase content. However, the diffraction patterns at the 0° sector, which is parallel to the electric field direction, can be used to quantify the domain switching fraction and lattice strains [17,32,33].

Figure 1(a) and 1(b) shows the $\{200\}_{pc}$ profiles of PT-36BS and PT-62BMT at the 0º sector as function of electric field. It is interesting to find the domain switching fractions to be almost the similar for both PT-36BS and PT-62BMT, even though they have much difference piezoelectric performance. Increasing the electric field results in texture, as a result of which the intensity of the $(002)_T$ reflection increases, while that of the $(200)_T$ decreases. The character of ferroelectric domain texture can be quantified by the multiple of random distribution ($f_{002,T}$) [40] (Fig. S3a and S5 of Ref. [25]). With increasing electric field, the $f_{002,T}$ value increases, indicating that larger fraction of the domains switch in response to the applied electric field. To estimate the mobility of domain wall, the ratio of $\Delta f_{002,T}/E$ [32,36] is calculated [Fig. 1(c)]. It is interesting to find that both MPB piezoceramics have similar domain wall mobility, as indicated by the remarkable approximate values of $\Delta f_{002,T}/E$ [0.10/(kV·mm^{-1})]. It suggests that the origin of the difference in piezoelectric performance of both the MPB piezoceramics is not dominated by domain switching but by other mechanisms. Furthermore, lower domain switching fractions have been observed in other high performance MPB ceramics, such as soft PZT [$\Delta f_{002,T}/E$ = 0.11/(kV·mm^{-1}), d_{33} = 500 pC/N], and $PbTiO_3$-$Bi(Ni_{1/2}Zr_{1/2})O_3$ [$\Delta f_{002,T}/E$ = 0.10/(kV·mm^{-1}), d_{33} = 390 pC/N] [41].

The lattice strain for both the MPB piezoceramics obtained at the 0º sector is shown in the Fig. S7 of Ref. [25]. As anticipated, the high performance PT-36BS exhibits larger lattice strains as opposed to PT-62BMT. The lattice strain evaluated from the $\{111\}_{pc}$ profile of PT-36BS (0.25% at 5 kV/mm, d^*_{33} = 500 pm/V) is higher in comparison to PT-62BMT (0.14% at 5 kV/mm, d^*_{33} = 260 pm/V). As shown in Fig. S2 of Ref. [25], a similar macrostrain property is also observed in ceramics of PT-36BS (0.29%) and PT-62BMT (0.14%). Note that the strain of $\{111\}_{pc}$ would result from the intergranular strain due to comprehensive factors of domain switching, phase coexistence and so on [42].

Why is there the prominent difference in piezoelectric performance despite the similar domain switching behavior in PT-36BS and PT-62BMT? As shown in Fig. 1(d) and 1(e), the compositions exhibit a stark difference in the $\{200\}_{pc}$ profiles of

the 45º sector. An electric-field-driven phase transformation occurs to a large extent in the high performance PT-36BS piezoceramics, while it is limited in the inferior PT-62BMT. With increasing electric field, the intensity of the shoulder peaks corresponding to the tetragonal (T) phase decreases, while the middle peaks of the second phase increases. In order to evaluate the phase fraction as function of electric field, the $\{200\}_{pc}$ profile is fitted to four peaks using pseudo-Voigt function (Fig. S4 of Ref. [25]). The T phase fraction (ξ_T) as a function of electric field for PT-36BS and PT-62BMT are contrasted in Fig. 1(f). Under application of electric field, the T phase fraction rapidly decreases for PT-36BS; however, this decrease is gradual in the case of PT-62BMT. This indicates that the interphase boundary mobility is enhanced in PT-36BS, but not in PT-62BMT. Perusing the above, the nature of the difference in the piezoelectric performance of PT-36BS and PT-62BMT can be attributed to the electric-field-driven phase transformation.

One can extend the above conclusion and argue if this is this indeed the general case for other MPB systems? In order to further confirm and expand the intrinsic correlation between piezoelectric performance and electric-field-driven phase transformation, we have investigated several other MPB piezoceramics exhibiting different degree of piezoelectric performance. The superior ones are La,Sr-doped $Pb(Zr_{0.53}Ti_{0.47})O_3$ (La,Sr-PZT, d_{33} = 500 pC/N), and $0.6PbTiO_3$-$0.4Bi(Ni_{1/2}Zr_{1/2})O_3$ (PT-40BNZ, d_{33} = 390 pC/N) [41], and the moderate ones are $0.57PbTiO_3$-$0.43Bi(Mg_{1/2}Zr_{1/2})O_3$ (PT-43BMZ, d_{33} = 300 pC/N) [43], and commercial PZT-4 ceramic (PZT-4, d_{33} = 289 pC/N). The evolution of the $\{200\}_{pc}$ profiles as a function of electric field at the 45º sector is depicted in Fig. S10 of Ref. [25]. It can be clearly seen that the middle bulge in the $\{200\}_{pc}$ profiles responds to electric field for those compositions, which is significant in the compositions with superior piezoelectric performance, but exhibits negligible/weak change for the compositions with moderate performance. It is worth noting that such phase transformation is reversible (Fig. S11 of Ref. [25]). Under loading a bipolar electric field, the T phase fraction displays a butterfly shape (Fig. S12 of Ref. [25]). Fig. 2(a) depicts the quantitative phase fractions of these piezoceramics as function of electric

field. Upon increasing electric field, the T phase fraction (ξ_T) gradually tapers off in all these ceramics, analogous to the previously reported soft PZT ceramics [16]. The T phase fractions exhibits a near linear relationship to electric field. Here, the slope defined as $d\xi_T/dE$ is adopted to indicate the tendency of phase transformation with respect to electric field. Larger value of $d\xi_T/dE$ signifies ease of phase transformation triggered by electric field. It is intriguing to observe a significant difference in $d\xi_T/dE$ for these piezoelectric systems. Larger values of $d\xi_T/dE$ are observed for La,Sr-PZT [4.8 %/(kV·mm^{-1})], PT-36BS [4.2 %/(kV·mm^{-1})], and PT-40BNZ [3.8 %/(kV·mm^{-1})], while the values are lower for PT-43BMZ [2.6 %/(kV·mm^{-1})] PZT-4 [2.61 %/(kV·mm^{-1})], and PT-62BMT [1.2 %/(kV·mm^{-1})]. The plot of d_{33} as function of $d\xi_T/dE$ [Fig. 2(b)] reveals an intriguing correlation. The piezoelectric performance is highly and directly correlated with the tendency of phase transformation. Larger value of $d\xi_T/dE$, higher the piezoelectric coefficient d_{33}. A large value of $d\xi_T/dE$ implies that smaller electric field amplitudes are sufficient to drive the phase transformation, resulting in ease of electric-field-driven phase transformation. This trend is also robust if extrapolating the line to the point of $d\xi_T/dE = 0$, in which corresponds to a single T phase. It indicates that pure T phase compositions have inferior piezoelectric properties as is the case in PT-30BS (130 pC/N) [44], La-doped $PbZr_{0.4}Ti_{0.6}O_3$ (130 pC/N) [45], PT-47BNT (180 pC/N) [46], and PT-60BMT (145 pC/N) [47]. It is unambiguous that d_{33} strongly correlates with $d\xi_T/dE$. Similarly, the large-signal d_{33} is strongly correlated with $d\xi_T/dE$ (Fig. S13 of Ref. [25]). The near-linear behavior suggests that the electric-field-driven phase transformation is the dominant contributing factor to the enhanced piezoelectric properties at the MPB.

Phase-field modelling was performed to investigate the general role of electric-field-driven phase transformation to enhance piezoelectric performance (details are provided in Supplemental Material [25]). For the domain configuration depicted in Fig. 3(a), the domains can be switched with electric field. It is the so called 90º domain switching. However, for the domain configuration shown in the left panel of Fig. 3(b), this state is stable if no phase transition occurs. In such case,

non-180º switching cannot occur under applied electric field and strain is low. Nevertheless, since the composition is at the MPB with coexisting phases that are energetically equivalent, it readily undergoes phase transformation upon application of electric field. Once the phase transformation is triggered by the electric field, the state will be overcome [Fig. 3(b)]. As the phase transformation occurs, the polarization tends to align along the electric field direction. The nucleation of the new phase are likely occurs at the domains walls based on the present and previous phase-field simulation results [48], which is in conjunction with the phase boundary motions to the T phase. The phase transformation enables the polarization to align along electric field to a larger extent [Fig. 3(d)]. Therefore, the phase transformation promotes some "death domains" active. The phase-field simulation [Fig. 3(c) and Fig. S14 of Ref [25]] indicates that under applied electric field, negligible phase transformation is observed for the non-MPB composition of T phase, which exhibits low piezoelectric response (d_{33}^{*} = 360 pm/V). For the PZT composition near MPB, it exhibits a moderate electric-field-driven phase transformation, and displays a moderate piezoelectric response (d_{33}^{*} = 560 pm/V). However, for the MPB composition, it exhibits enhanced electric-field-driven phase transformation, and high piezoelectric performance (d_{33}^{*} = 640 pm/V). Coinciding with the in-situ high-energy SXRD results, the phase-field modelling also reveals that a high tendency of phase transformation driven by electric field generates a high piezoelectric response. The piezoelectric response is, therefore, improved by the enhanced polarization alignment [49], and additional interphase boundary motion.

Similarly, when electric field is applied along the <001> direction of rhombohedral PZN-PT crystals, strain abruptly increases, which is associated with electric-field-driven R to T phase transformation and the inclined polarization jump to the electric field direction [4]. According to the Landau-Ginsburg-Devonshire (LGD) thermodynamic theory [22], the high sensitivity of phase transformation to electric field can be interpreted as a flattening of the anisotropic free energy profiles. A flatter free energy profile suggests an enhanced susceptibility of atomic displacements, and thus gives rise to enhanced piezoelectricity.

In general, the major contributing factors to the piezoelectric performance are domain switching, lattice strain and phase transformation. The extrinsic contribution can be maximized though domain engineering [4,50]. The intrinsic structure-related contribution can be largely promoted by flexible continuous polarization rotation via single monoclinic structure [33,39,51,52]. For the MPB piezoceramics, the high piezoelectric performance can be achieved via the enhancement of reversible phase transformation by optimizing extrinsic factors, such as grain size, and domain wall density.

In summary, the evolution of lattice strain, domain switching, and in particular, phase transformation have been evaluated using in-situ high-energy SXRD under applied electric field in various perovskite-type piezoelectric systems. The results provide a direct experimental evidence that the electric-field-driven phase transformation plays a dominant role in the piezoelectric performance of MPB compositions. A strong tendency of electric-field-driven phase transformation generates a peak piezoelectric response. The polarization alignment can be enhanced via the electric-field-driven phase transformation. The present results will inspire insight for functional materials whose properties are related to external-stimuli-driven phase transformation such as ferroelectrics, ferromagnets, and ferroelastics.

This work was supported by the National Natural Science Foundation of China (Grant Nos. 91422301, 21231001, 21590793 and 11504020), National Program Support of Top-notch Young Professionals, and Program for Chang Jiang Young Scholars, and the Fundamental Research Funds for the Central Universities, China. This research used resources of the Advanced Photon Source, a U.S. Department of Energy (DOE) Office of Science User Facility operated for the DOE Office of Science by Argonne National Laboratory under Contract No. DE-AC02-06CH11357. L.-Q. C. is supported by the U.S. Department of Energy, Office of Basic Energy Sciences, Division of Materials Sciences and Engineering under Award DE-FG02-07ER46417. We thank Dr. K. V. Lalitha and H. Zhou for the helpful

discussions.

References

[1] J. Zeches, M. D. Rossell, J. X. Zhang, A. J. Hatt, Q. He, C. H. Yang, A. Kumar, C. H. Wang, A. Melville, C. Adamo, G. Sheng, Y. H. Chu, J. F. Ihlefeld, R. Erni, C. Ederer, V. Gopalan, L. Q. Chen, D. G. Schlom, N. A. Spaldin, L. W. Martin, and R. Ramesh, Science **326**, 977 (2009).

[2] M. Ahart, M. Somayazulu, R. E. Cohen, P. Ganesh, P. Dera, H. K. Mao, R. J. Hemley Y. Ren, and Z. Wu, Nature **451**, 545 (2008).

[3] S. Yang, H. Bao, C. Zhou, Y. Wang, X. Ren, Y. Matsushita, Y. Katsuya, M. Tanaka, K. Kobayashi, X. Song, and J. Gao, Phys. Rev. Lett. **104**, 197201 (2010).

[4] S. E. Park, and T. R. Shrout, J. Appl. Phys. **82**, 1804 (1997).

[5] J. X. Zhang, B. Xiang, Q. He, J. Seidel, R. J. Zeches, P. Yu, S. Y. Yang, C. H. Wang, Y. H. Chu, L. W. Martin, A. M. Minor, and R. Ramesh, Nat. Nanotech. **6**, 98 (2011).

[6] R. Kainuma, Y. Imano, W. Ito, Y. Sutou, H. Morito, S. Okamoto, O. Kitakami, K. Oikawa, A. Fujita, T. Kanomata, and K. Ishida, Nature **439**, 957 (2006).

[7] M. Chmielus, X. X. Zhang, C. Witherspoon, D. C. Dunand, and P. Mullner, Nat. Mater. **8**, 863 (2009).

[8] J. Liu, T. Gottschall, K. P. Skokov, J. D. Moore, and O. Gutfleisch, Nat. Mater. **11**, 620 (2012).

[9] X. Tan, J. Frederick, C. Ma, W. Jo, and J. Rödel, Phys. Rev. Lett. **105**, 255702 (2010).

[10] D. A. Ochoa, G. Esteves, J. L. Jones, F. Rubio-Marcos, J. F. Fernández, and J. E. García, Appl. Phys. Lett. **108**, 142901 (2016).

[11] B. Jaffe, W. R. Cook, and H. Jaffe, London, Piezoelectric Ceramics (Academic Press, New York, 1971).

[12] G. H. Haertling, J. Am. Ceram. Soc. **82**, 797 (1999).

[13] Z. Wu, and R. E. Cohen, Phys. Rev. Lett. **95**, 037601 (2005).

[14] S. Zhang, F. Li, X. Jiang, J. Kim, J. Luo, and X. Geng, Prog. Mater. Sci. **68**, 1 (2015).

[15] K. Shimizu, H. Hojo, Y. Ikuhara, and M. Azuma, Adv. Mater. **28**, 8639 (2016).

[16] M. Hinterstein, J. Rouquette, J. Haines, P. Papet, M. Knapp, J. Glaum, and H. Fuess, Phys. Rev. Lett. **107**, 077602 (2011).

[17] D. K. Khatua, Lalitha K. V., C. M. Fancher, J. L. Jones, and R. Ranjan, Phys. Rev. B **93**, 104103 (2016).

[18] C. Ma, H. Guo, S. P. Beckman, and X. Tan, Phys. Rev. Lett. **109**, 107602 (2012).

[19] J. E. Daniels, W. Jo, J. Rödel, and J. L. Jones, Appl. Phys. Lett. **95**, 032904 (2009).

[20] J. E. Daniels, W. Jo, J. Rödel, V. Honkimäki, and J. L. Jones, Acta Mater **58**, 2103 (2010).

[21] D. Damjanovic, Appl. Phys. Lett. **97**, 062906 (2010).

[22] D. Damjanovic, J. Am. Ceram. Soc. **88**, 2663 (2005).

[23] B. Noheda, D. E. Cox, G. Shirane, S. E. Park, L. E. Cross, and Z. Zhong, Phys. Rev. Lett. **86**, 3891 (2001).

[24] M. Hinterstein, M. Hoelzel, J. Rouquette, J. Haines, J. Glaum, H. Kungl, and M. Hoffman, Acta Mater. **94**, 319 (2015).

[25] See Supplemental Material at http://link.aps.org/supplemental/ for details of materials synthesis, experimental setup, data processing, phase field simulation, and supporting figures and tables, which includes Refs. [26–31].

[26] G. Tutuncu, D. Damjanovic, J. Chen, and J. L. Jones, Phys. Rev. Lett. **108**, 177601 (2012).

[27] G. Tutuncu, J. Chen, L. L. Fan, C. M. Fancher, J. S. Forrester, J. Zhao, J. L. Jones, J. Appl. Phys. **120**, 044103 (2016).

[28] H. Toraya, M. Yoshimura and S. Somiya, J. Am. Ceram. Soc. **67**, 6 (1984).

[29] L. Q. Chen, J. Am. Ceram. Soc. **91**, 1835 (2008).

[30] Y. Cao, G. Sheng, J. X. Zhang, S. Choudhury, Y. L. Li, C. A. Randall1, and L. Q. Chen, Appl. Phys. Lett. **97**, 252904 (2010).

[31] L. Q. Chen, and J. Shen, Comput. Phys. Commun. **108**, 147 (1998).

[32] L. L. Fan, J. Chen, Y. Ren, Z. Pan, L. X. Zhang, and X. R. Xing, Phys. Rev. Lett. **116**, 027601 (2016).

[33] H. Liu, J. Chen, L. L. Fan, Y. Ren, Z. Pan, K.□V. Lalitha, J. Rödel, and X. R. Xing, Phys. Rev. Lett. **119**, 017601 (2017).

[34] D. A. Ochoa, G. Esteves, T. Iamsasri, F. Rubio-Marcos, J. F. Fernández, J. E. Garcia, and J. L. Jones, J. Eur. Ceram. Soc. **36** 2489 (2016).

[35] T. Leist, T. Granzow, W. Jo, and J. Rödel, J. Appl. Phys. **108**, 014103 (2010).

[36] G. Tutuncu, B. Li, K. Bowman, and J. L. Jones, J. Appl. Phys. **115**, 144104 (2014).

[37] R. E. Eitel, C. A. Randall, T. R. Shrout, P. W. Rehrig, W. Hackenberger, and S. E. Park, Jpn. J. Appl. Phys. **40**, 5999 (2001).

[38] J. Chen, W. Jo, X. Tan, and J. Rödel, J. Appl. Phys. **106**, 034109 (2009).

[39] H. Liu, J. Chen, L. L. Fan, Y. Ren, L. Hu, F. M. Guo, J. X. Deng, and X. R. Xing, Chem. Mater. **29**, 5767 (2017).

[40] J. L. Jones, E. B. Slamovich, and K. J. Bowman, J. Appl. Phys. **97**, 034113 (2005).

[41] Y. C. Rong, J. Chen, H. J. Kang, L. J. Liu, L. Fang, L. L. Fan, Z. Pan, and X. R. Xing, J. Am. Ceram. Soc. **96**, 1035 (2013).

[42] Lalitha K. V., C. M. Fancher, J. L. Jones, and R. Ranjan, Appl. Phys. Lett. **107**, 052901 (2015).

[43] L. L. Fan, J. Chen, Q. Wang, J. X. Deng, R. B. Yu, and X. R. Xing, Ceram. Int. **40**, 7723 (2014).

[44] Lalitha K. V., A. N. Fitch, and R. Ranjan, Phys. Rev. B **87**, 064106 (2013).

[45] A. Pramanick, D. Damjanovic, J. E. Daniels, J. C. Nino, and J. L. Jones, J. Am. Ceram. Soc. **94**, 293 (2011).

[46] S. M. Choi, C. J. Stringer, T. R. Shrout, and C. A. Randall, J. Appl. Phys. **98**, 34108 (2005).

[47] C. A. Randall, R. Eitel, B. Jones, T. R. Shrout, D. I. Woodward, and I. M. Reaney, J. Appl. Phys. **95**, 3633 (2004).

[48] Y. U. Wang, J. Mater. Sci. **44**, 5225 (2009).

[49] J. Y. Li, R. C. Rogan, E. Üstündag, and K. Bhattacharya, Nat. Mater. **4**, 776 (2005).

[50] S. E. Park, S. Wada, L. E. Cross, and T. R. Shrout, J. Appl. Phys. **86**, 2746 (1999).

[51] H. Fu, and R. E. Cohen, Nature **403**, 281 (2000).

[52] K. Oka, T. Koyama, T. Ozaaki, S. Mori, Y. Shimakawa, and M. Azuma, Angew. Chem., Int. Ed. Engl. **51**, 7977 (2012).

FIG. 1. Diffraction peak profiles and contour plots of $\{200\}_{pc}$ as function of electric field at the 0º and 45º sectors, (a) PT-36BS and (b) PT-62BMT at the 0º sector, (d) PT-36BS and (e) PT-62BMT at the 45º sector. The blue arrows indicate the direction of increasing electric field amplitude. (c) Electric-field-dependent $\Delta f_{002,T}$ of PT-36BS and PT-62BMT ceramics obtained from the 0º sector. (f) The electric field dependence of tetragonal phase fraction (ξ_T) for PT-36BS and PT-62BMT ceramics obtained from the 45º sector.

FIG. 2. Strong correlation between piezoelectric performance and electric-field-driven phase transformation for various MPB compositions. (a) The T phase fraction as function of electric field (ξ_T *vs.* E). (b) The piezoelectric coefficient d_{33} as function of the $d\xi_T/dE$.

FIG. 3. (a) Normal polarization alignment via 90º domain switching. (b) Enhanced polarization alignment via electric-field-driven phase transformation. (c) The calculated piezoelectric strain from phase-field simulation for the PZT compositions of MPB, near MPB, and non-MPB T phase, which generates electric-field-driven high extent, moderate, and negligible phase transformation, respectively. (d) Polarization profile along the dash line.

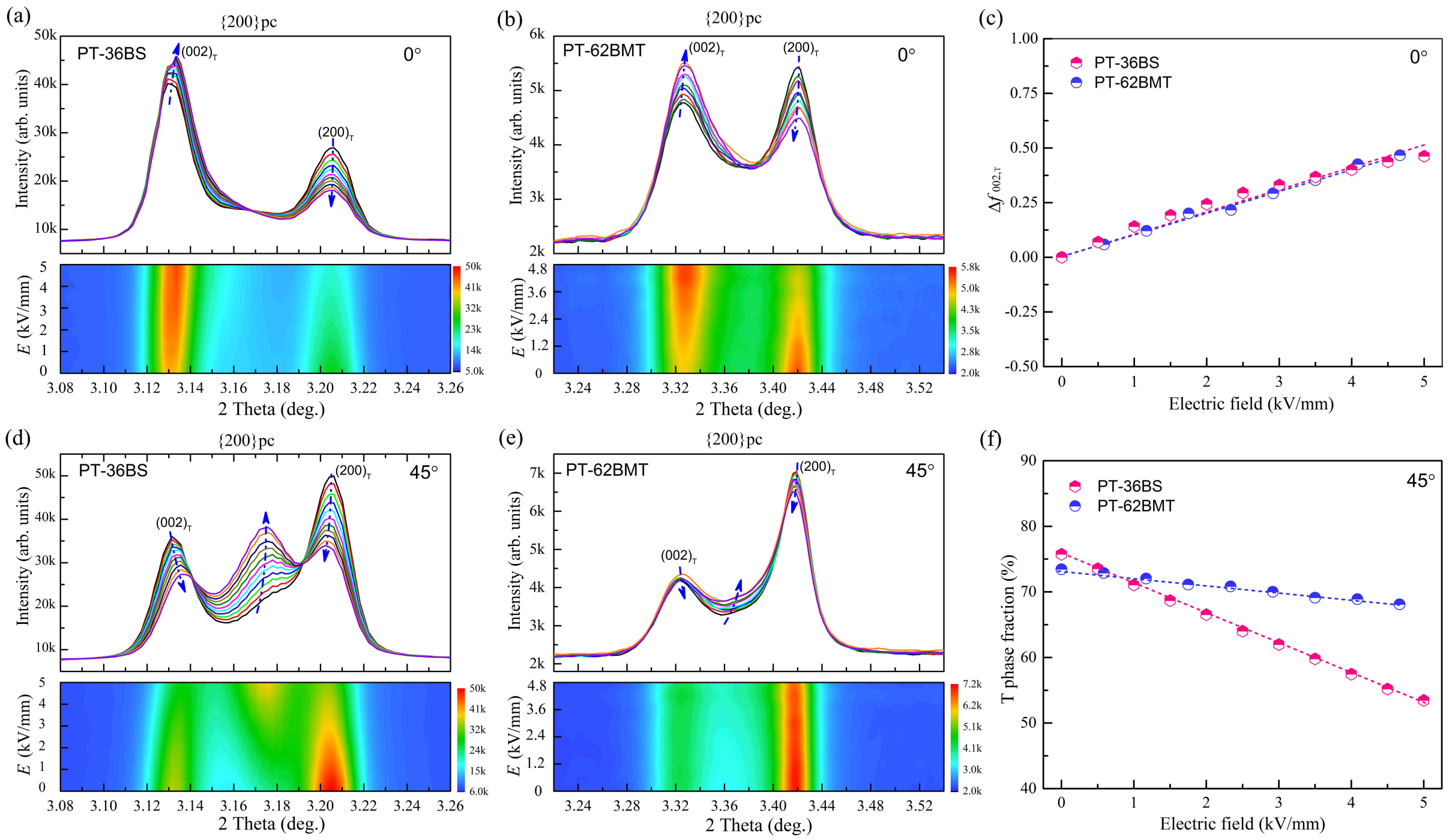
(a)
{200}pc
PT-36BS
0°
(002)T
(200)T
Intensity (arb. units)
E (kV/mm)
2 Theta (deg.)
(b)
{200}pc
PT-62BMT
0°
(002)T
(200)T
Intensity (arb. units)
E (kV/mm)
2 Theta (deg.)
(c)
PT-36BS
PT-62BMT
0°
Δf 002,T
Electric field (kV/mm)
(d)
{200}pc
PT-36BS
45°
(002)T
(200)T
Intensity (arb. units)
E (kV/mm)
2 Theta (deg.)
(e)
{200}pc
PT-62BMT
45°
(002)T
(200)T
Intensity (arb. units)
E (kV/mm)
2 Theta (deg.)
(f)
PT-36BS
PT-62BMT
45°
T phase fraction (%)
Electric field (kV/mm)

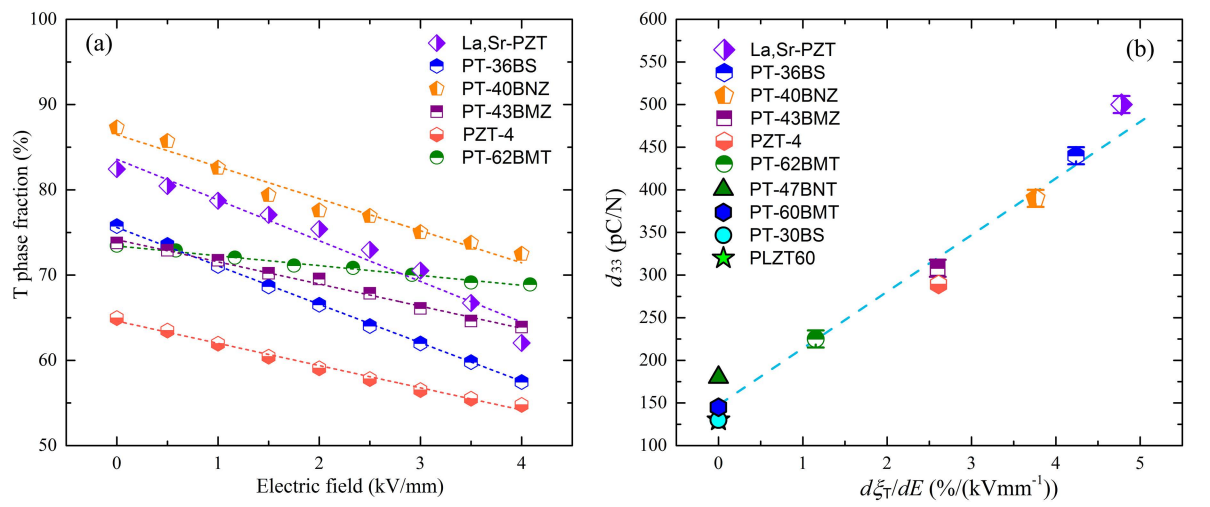
(a)
La,Sr-PZT
PT-36BS
PT-40BNZ
PT-43BMZ
PZT-4
PT-62BMT
T phase fraction (%)
Electric field (kV/mm)
(b)
La,Sr-PZT
PT-36BS
PT-40BNZ
PT-43BMZ
PZT-4
PT-62BMT
PT-47BNT
PT-60BMT
PT-30BS
PLZT60
d_{33} (pC/N)
$d\xi_T/dE$ (%/(kVmm^{-1}))

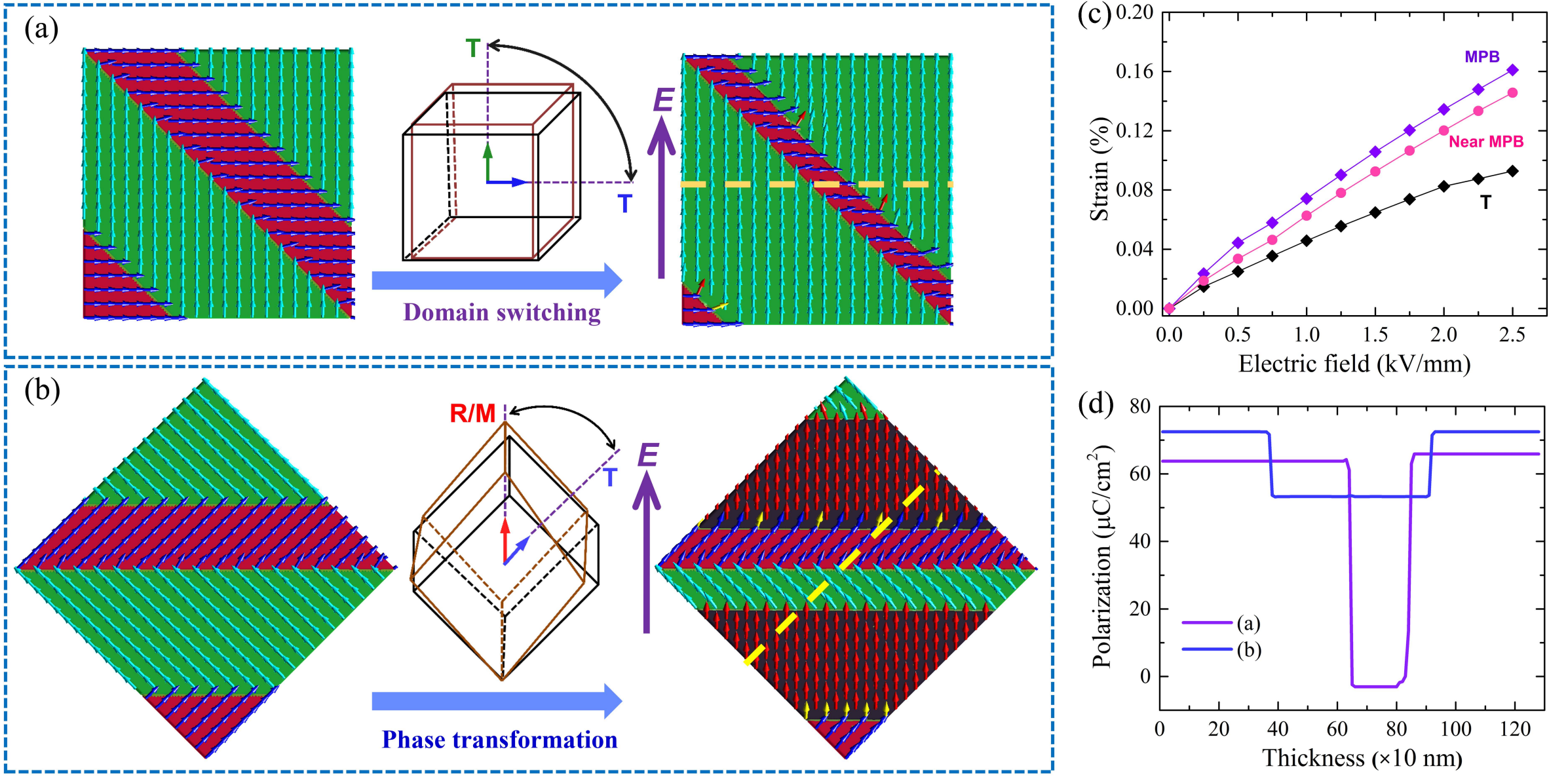
(a)
T
T
E
Domain switching
(b)
R/M
T
E
Phase transformation
(c)
MPB
Near MPB
T
Strain (%)
0.00
0.04
0.08
0.12
0.16
0.20
0.0
0.5
1.0
1.5
2.0
2.5
Electric field (kV/mm)
(d)
Polarization (μC/cm²)
80
60
40
20
0
(a)
(b)
0
20
40
60
80
100
120
Thickness (×10 nm)